

Orbital and Mass Ratio Evolution of Protobinaries Driven by Magnetic Braking

Bo Zhao¹, Zhi-Yun Li¹

ABSTRACT

The majority of stars reside in multiple systems, especially binaries. The formation and early evolution of binaries is a longstanding problem in star formation that is not yet fully understood. In particular, how the magnetic field observed in star-forming cores shapes the binary characteristics remains relatively unexplored. We demonstrate numerically, using an MHD version of the ENZO AMR hydro code, that a magnetic field of the observed strength can drastically change two of the basic quantities that characterize a binary system: the orbital separation and mass ratio of the two components. Our calculations focus on the protostellar mass accretion phase, after a pair of stellar “seeds” have already formed. We find that, in dense cores magnetized to a realistic level, the angular momentum of the material accreted by the protobinary is greatly reduced by magnetic braking. Accretion of strongly braked material shrinks the protobinary separation by a large factor compared to the non-magnetic case. The magnetic braking also changes the evolution of the mass ratio of unequal-mass protobinaries by producing material of low specific angular momentum that accretes preferentially onto the more massive primary star rather than the secondary. This is in contrast with the preferential mass accretion onto the secondary previously found numerically for protobinaries accreting from an unmagnetized envelope, which tends to drive the mass ratio towards unity. In addition, the magnetic field greatly modifies the morphology and dynamics of the protobinary accretion flow. It suppresses the traditional circumstellar and circumbinary disks that feed the protobinary in the non-magnetic case; the binary is fed instead by a fast collapsing pseudodisk whose rotation is strongly braked. The magnetic braking-driven inward migration of binaries from their birth locations may be constrained by high-resolution observations of the orbital distribution of deeply embedded protobinaries, especially with ALMA and JVLA.

Subject headings: binary, accretion disks — magnetic fields — stars: formation — magnetohydrodynamics (MHD)

¹University of Virginia, Astronomy Department, Charlottesville, USA

1. Introduction

The majority of the Galactic field stars reside in multiple systems (Duquennoy & Mayor 1991; Fischer & Marcy 1992; Mason et al. 1998; Shatsky & Tokovinin 2002; Goodwin & Kroupa 2005; Raghavan et al. 2010; Janson et al. 2012); most of those systems ($\sim 75\%$) are binaries (Duquennoy & Mayor 1991; Tokovinin & Smekhov 2002). The multiplicity of young stellar objects is even higher (Reipurth & Zinnecker 1993; Mathieu et al. 2000; Duchêne et al. 2004; Duchêne et al. 2007), indicating that the formation of multiple systems, especially binaries, is a major, perhaps the dominant, mode of star formation.

How binaries form and evolve remains uncertain. This is particularly true for the earliest, Class 0, phase, when the stellar seeds are still deeply embedded inside a massive envelope. Although millimeter interferometric observations such as Looney et al. (2000) have uncovered some Class 0 binaries, their number is still small, and the distribution of orbital separation of such protobinaries is not well constrained. Maury et al. (2010) surveyed 5 Class 0 sources with PdBI at sub-arcsecond resolution, and found a surprising result: only one of the sources has a potential protostellar companion, and the companion is $\sim 1,900$ AU away from the primary. Combining their sample with that of Looney et al. (2000), Maury et al. (2010) found that none of the 14 Class 0 sources in the combined sample has a companion with separation between $\sim 150 - 550$ AU, which is inconsistent with the binary fraction of $\sim 18\%$ for Class I sources in the same separation range (Connelley et al. 2008). A similar difference was found in the CARMA survey of 6 Class 0 and 3 Class I sources in the Serpens molecular cloud (Enoch et al. 2011). None of the Class 0 objects has any detectable protostellar companion closer than $2,000$ AU (down to the resolution limit ~ 250 AU), whereas one Class I object has a companion at a projected distance of ~ 870 AU. Although the statistical significance of the difference is still relatively low, it brings into sharp focus the possibility that the distribution of orbital separation of protobinaries may differ significantly from that of their more mature counterparts. In other words, binaries may migrate substantially from their birth locations, a situation somewhat analogous to that inferred for hot Jupiters, although it is unclear whether protobinaries would migrate inward or outward to fill the apparent gap between $\sim 150 - 550$ AU. The direction (inward vs outward) of protobinary orbital migration should be better constrained observationally with large surveys of deeply embedded sources using ALMA and JVLA.

This paper focuses on one possible mechanism for moving the protobinaries away from their birth locations: magnetic braking. It may seem counter-intuitive that magnetic fields can change the binary orbit, because the magnetic forces do not act on the stars directly. However, the orbits of protobinaries are determined mainly by the angular momentum of the material to be accreted, which can be strongly affected, perhaps even controlled, by

the magnetic field, through magnetic braking. The main goal of this paper is to quantify the extent to which the protobinary orbit is modified by a magnetic field of the observed strength.

The strength of magnetic fields in star formation is usually measured by the dimensionless mass-to-flux ratio λ . It is the mass of a region divided by the magnetic flux threading the region in units of the critical value $(2\pi G^{1/2})^{-1}$ (Nakamura & Nakano 1978). For a sample of dense cores in the nearby dark clouds, Troland & Crutcher (2008) inferred a mean value for $\lambda_{los} \sim 4.8$, based on the field strength and column density along the line-of-sight. Geometric corrections for projection effects should reduce this value by a factor of 2-3, yielding an intrinsic value of λ of a few typically. Such a magnetic field is generally not strong enough to prevent the dense core from gravitational collapse and star formation. It is, however, strong enough to affect the angular momentum evolution of the collapsing core in general and binary formation in particular.

There have been several studies of the magnetic effects on binary formation (e.g., Price & Bate 2007; Hennebelle & Teyssier 2008; Machida et al. 2010). These studies focused primarily on the classical mode of binary formation inside an isolated rotating core, through core fragmentation induced by an $m = 2$ density perturbation (e.g., Boss & Bodenheimer 1979, see Kratter 2011 for a recent review). A general conclusion is that the fragmentation can be suppressed by a rather weak magnetic field if the core is only weakly perturbed. For example, Hennebelle & Teyssier 2008 found that, for a density perturbation of 10%, the fragmentation is suppressed by a magnetic field corresponding to $\lambda = 20$ (see their Fig. 3), much weaker than the observationally inferred field. In dense cores that are magnetized to a more realistic level (with $\lambda \sim$ a few), fragmentation can still occur, although a large amplitude perturbation is needed (Price & Bate 2007; Hennebelle & Teyssier 2008). A limitation of the existing MHD calculations is that they are confined mostly to the pre-stellar phase of core collapse and fragmentation leading up to the formation of two binary seeds. How the binary seeds evolve during the subsequent protostellar mass accretion phase in the presence of a dynamically important magnetic field remains little explored. It is the focus of our investigation.

Our investigation of the magnetic effects on protobinary evolution will be carried out using an MHD version of the ENZO AMR hydro code that includes a sink particle treatment (Bryan & Norman 1997; O’Shea et al. 2004; Wang & Abel 2009; Wang et al. 2010). In § 2, we discuss the setup for the initial binary seeds and the rotating magnetized protobinary envelope to be accreted by the seeds, as well as the numerical code used. In § 3, we present numerical results for the evolution of initially equal-mass binary seeds. We find that a magnetic field of the observed strength can shrink the protostellar orbit by more than an

order of magnitude compared to the non-magnetic case. It also greatly changes the dynamics and morphology of the protostellar accretion flow near the binary. For initially unequal mass binary seeds, the issue of mass ratio evolution becomes important. In § 4, we follow the evolution of unequal-mass protobinaries accreting from envelopes magnetized to different levels. We find that the well-known tendency towards equal mass in the non-magnetic case due to preferential mass accretion onto the secondary is weakened or even suppressed by magnetic braking. We summarize the main results and put them in context in § 5.

2. Problem Setup

As mentioned in the introduction, the focus of our investigation is on the protostellar accretion phase of binary formation, where the magnetic effects are least explored. We will therefore skip the pre-stellar phase of core evolution leading up to the production of a pair of binary seeds, and assume that, at the beginning of our calculations, the seeds are already formed and are ready to accrete from a rotating, magnetized envelope. The setup is similar in spirit to the influential work of Bate & Bonnell (1997) and Bate (2000), who studied the effects on binary properties of mass accretion from an unmagnetized envelope (see also Artymowicz 1983). We postpone a treatment of both the pre-stellar and protostellar phases of binary formation to a future investigation. In what follows, we describe the initial conditions for the envelope and binary seeds as well as the numerical code used for following the envelope collapse and protobinary accretion.

Although protostellar envelopes are often observed to be irregular and filamentary (e.g., Tobin et al. 2010), it is instructive to model them simply, so that the basic effects can be illustrated as cleanly as possible. Since the formation and evolution of binaries involve complex dynamics that are challenging to simulate and interpret, it is useful to set up the calculations in such a way that the numerical results can be checked against analytic expectations. One way to achieve this is to start with a self-similar initial configuration for the envelope, with an r^{-2} density distribution given by (Shu 1977)

$$\rho(r) = \frac{Ac_s^2}{4\pi Gr^2}, \quad (1)$$

where c_s is the isothermal sound speed, and A is an over-density parameter. The collapse of such an initial configuration is expected to remain self-similar (Shu 1977), and the self-similarity has proven to provide a powerful check on the numerically obtained solutions (see, e.g., Allen et al. 2003; Mellon & Li 2008; 2009; Kratter et al. 2010; and discussion in § 3).

We choose an over-density parameter $A = 4$ (corresponding to a ratio of thermal to gravitational energy of $\alpha = 3/(2A) = 0.375$), so that the initial configuration is denser than

the famous equilibrium singular isothermal sphere by a factor of 2. The mass enclosed within any radius r can be integrated as,

$$M(r) = \frac{Ac_s^2}{G}r. \quad (2)$$

For an adopted core radius $R = 10^{17}$ cm and isothermal sound speed $c_s = 0.2$ km/s (corresponding to a temperature of ~ 10 K), the above equation yields a total core mass $M_{tot} = 1.2 M_\odot$ and an average free-fall time $t_{ff} \approx 88$ kyr.

We generalize the isothermal configuration to include both rotation and magnetic fields. To preserve the self-similarity, the rotation speed cannot depend on radius but can have an angular dependence (Allen et al. 2003). A convenient choice is $v_\phi = v_0 \sin \theta$ (where θ is the polar angle measured from the rotation axis), which ensures that the angular speed is finite on the axis. We pick $v_0 = c_s$, in order to have as large a rotation speed as possible, so that the binary can be well resolved, especially for strongly magnetized cases where the binary separation is reduced by a large factor compared to the non-magnetic case; even faster, supersonic, rotation may produce undesirable shocks. The adopted rotation profile corresponds to a ratio of rotational to gravitational energy $\beta = (v_0/c_s)^2/(3A) \approx 0.083$, somewhat higher than used in other works (e.g., Machida et al. 2010). Nonetheless, it is still within the range inferred by Goodman et al. (1993) from NH_3 observations of dense cores.

We choose an initially uni-directional magnetic field along the rotation axis (or the z -axis in the simulations), with the field strength decreasing away from the axis as $1/\varpi$ (where ϖ is the cylindrical radius), such that the mass-to-flux ratio is constant spatially. To avoid singularity at the origin, we soften the profile to $1/(\varpi + r_h)$, so that

$$B_z(\varpi) = \frac{Ac_s^2}{\sqrt{G\lambda}} \frac{1}{\varpi + r_h}, \quad (3)$$

where λ in the denominator is the dimensionless mass-to-flux ratio of the envelope in units of the critical value $(2\pi G^{1/2})^{-1}$, and the parameter r_h is defined below. Even though dense cores typically have λ of a few (see discussion in § 1), we will consider a much wider range of $\lambda = 2, 4, 8, 16$ and 32 , as well as the non-magnetic case ($\lambda = \infty$), so as to capture any trend that may exist in the protobinary properties as the field strength increases gradually.

To study the protobinary evolution, we follow Bate & Bonnell (1997) and Bate (2000) and insert two equal-mass “seeds” near the center of the protostellar envelope at the beginning of the calculation; non-equal mass binaries will be treated separately in § 4. We assume that each of the binary seeds has a small initial mass of $0.05 M_\odot$. To determine the initial binary separation, we assume that the binary seeds get both their masses and orbital angular momentum from a sphere of radius $r_h = 8.30 \times 10^{15}$ cm in the initial envelope that contains $0.1 M_\odot$. In other words, we assign both the mass and angular momentum inside r_h

to the binary seeds. The initial orbital angular momentum is thus

$$L_b = L(r_h) = \int_0^{r_h} \int_0^\pi \int_0^{2\pi} \rho v_0 \sin \theta \varpi r^2 \sin \theta \, dr d\theta d\phi = \frac{Ac_s^2 v_0}{3G} r_h^2, \quad (4)$$

which, for circular orbits, yields an initial binary separation of

$$a = \frac{16A^2 c_s^4 v_0^2 r_h^4}{9(GM_b)^3} = 3.687 \times 10^{15} \text{ cm} \approx 246 \text{ AU}, \quad (5)$$

where $M_b = 0.1 M_\odot$ is the total mass of the binary.

To follow the envelope accretion and protobinary evolution, we use an MHD version (Wang & Abel 2009) of the ENZO adaptive mesh refinement hydro code (Bryan & Norman 1997; O’Shea et al. 2004). It incorporates a sink particle treatment (Wang et al. 2010). The magnetic field is evolved with a conservative MHD solver that includes the hyperbolic divergence cleaning of Dedner et al. (2002). The MHD version of the code is publicly available from the ENZO website at <http://code.google.com/p/enzo/>. It has been used to follow successfully the formation and evolution of magnetized galaxies (Wang & Abel 2009) and star clusters (Wang et al. 2010), as well as single star formation in magnetized dense cores (Zhao et al. 2011).

We carry out simulations with periodic boundary conditions inside a box of length 5×10^{17} cm on each side, which is significantly larger than the protobinary envelope (of radius 10^{17} cm). The region outside the envelope is filled with a uniform isothermal medium of the same density (and temperature) as that at the outer boundary of the envelope ($\rho_a \approx 1.91 \times 10^{-19}$ g cm $^{-3}$), so that the pressures are initially balanced across the boundary. To speed up computation, we adopt a relatively coarse base grid of 64^3 , but allow for 8 levels of refinement, with a smallest cell size of about 2.0 AU.

As usual, we adopt a barotropic equation of state (EOS) that mimics the isothermal EOS at low densities and adiabatic EOS at high densities:

$$P(\rho) = \rho c_s^2 \left[1 + \left(\frac{\rho}{\rho_{crit}} \right)^{2/3} \right], \quad (6)$$

with a critical density $\rho_{crit} = 10^{-13}$ g cm $^{-3}$ for the transition between the two regimes.

We treat the binary stars as sink particles. The sink particle treatment is described in detail in Wang et al. 2010. Briefly, each particle accretes according to a modified Bondi-Hoyle formula (see Ruffert 1994). New sink particles are created at the center of those over-dense cells that violate the Jeans criterion at the highest refinement level, i.e. when

$\rho_{cell} > \rho_J = \frac{\pi}{G} \left(\frac{c_s}{N \Delta x} \right)^2 = 7.90 \times 10^{-14} g \cdot cm^{-3}$, where we have used a Truelove’s (Truelove et al. 1997) safety number $N = 16$ and a finest cell size $\Delta x = 3.05 \times 10^{13}$ cm. Newly created sink particles are subject to merging, which is controlled by two parameters: the merging mass $M_{merg} = 0.01 M_\odot$ and merging distance $l_{merg} = 5 \times 10^{14}$ cm (for details, see Wang et al. 2010). These values are chosen to eliminate artificial particles and to maximize computation efficiency. Our main results are insensitive to these parameters as long as they are reasonably small.

We have tested the sink particle accretion algorithm against known semi-analytic solutions of the collapse of (non-magnetic) singular isothermal sphere (Shu 1977) and found good agreement. For example, the collapse of our chosen initial configuration (Eq. [1] with $A = 4$) yields, after some initial adjustment, a constant mass accretion rate of $1.06 \times 10^{-5} M_\odot \text{ yr}^{-1}$, which matches Shu’s result almost exactly.

In a magnetized medium, we let the sink particle accrete only the mass but not the magnetic field; the field is left behind. This treatment is a crude representation of the decoupling of the magnetic field from the matter expected at high densities (Nakano et al. 2002; see discussion in Zhao et al. 2011).

3. Magnetic Braking and Protobinary Orbital Evolution

Before discussing detailed quantitative results, we first describe the qualitative effects of the magnetic field on the (initially equal-mass) protobinary orbit by contrasting the two extreme cases: the case without a magnetic field (the HD or hydro case hereafter), and the strongest field case ($\lambda = 2$, which is consistent with available Zeeman measurements, see Troland & Crutcher 2008). Both simulations reached a rather late time ($t \gtrsim 80$ kyr, comparable to the free-fall time at the average density), when the binary seeds have finished many orbits around each other. In Fig. 1, we show the snapshots of the two cases near the middle point of the simulation, at $t \approx 39$ kyr. They look strikingly different. In the HD case, there are two well separated stars, each surrounded by a circumstellar disk. The disks are surrounded by a well-defined circumbinary structure, with two prominent spiral arms embedded in it. The circumstellar disks and circumbinary structure are similar to those found in previous non-magnetic calculations, such as Bate (2000) and Hanawa et al. (2010). They are the result of the conservation of angular momentum in the rapid collapsing region of the envelope, and redistribution of angular momentum close to the binary through gravitational torque.

These well-known features are completely absent in the strongly magnetized $\lambda = 2$ case.

They are replaced by two irregular lobes, which were studied in detail in Zhao et al. (2011); they are the so-called “magnetic decoupling-enabled structures” (or DEMS for short) produced by the magnetic flux decoupled from the matter that enters the stars (sink particles). The DEMS are magnetically dominated, low-density, expanding regions. They surround the protobinary, whose separation is much smaller than that of the HD case (see Fig. 1). Clearly, the magnetic field has greatly modified not only the circumstellar and circumbinary structures, but also the binary orbit. In the following subsections, we will discuss these modifications more quantitatively.

3.1. Binary Separation and Angular Momentum-Mass Relation

3.1.1. *Hydro Case: Checking against Expectations*

We begin our quantitative discussion with binary separation. It is shown as a function of time in Fig. 2 for all initially equal-mass simulations. The evolution of the binary separation is particularly interesting in the HD case. It decreases initially for about 20 kyr, before increasing almost linearly with time¹. The linear increase is a natural consequence of the initial protostellar envelope configuration chosen, which is self-similar over a range of radii (excluding the regions close to the center and the outer edge). The configuration is expected to collapse self-similarly, with the binary separation increasing linearly with time (for the same reason that the size of the expansion wave in the well-known inside out collapse of a singular isothermal sphere increases linear with time; Shu 1977), after some initial adjustment. The decrease in binary separation during the initial adjustment comes about because we have put all of the angular momentum of the material inside a small sphere into the orbit of the initial binary seeds. This leads to an overestimate of the initial binary orbital angular momentum (and thus the separation) because a fraction of the angular momentum should be left behind in the circumstellar disks and circumbinary structure. We have experimented with binary seeds formed out of a smaller sphere that have smaller initial masses and separation. They exhibit a similar linear growth of separation with time after a shorter adjustment period. In other words, the protobinary reaches the expected self-similar state more quickly. The agreement of the numerical result with expectations gives us confidence that the ENZO-based AMR code can treat the protobinary evolution problem properly.

Another check on the numerical solution comes from the expected scaling between the

¹The wiggles on the curve is due to small orbital eccentricity (of order 10% or less) excited during the protobinary evolution. We will postpone a detailed study of the magnetic effect on eccentricity to a future investigation.

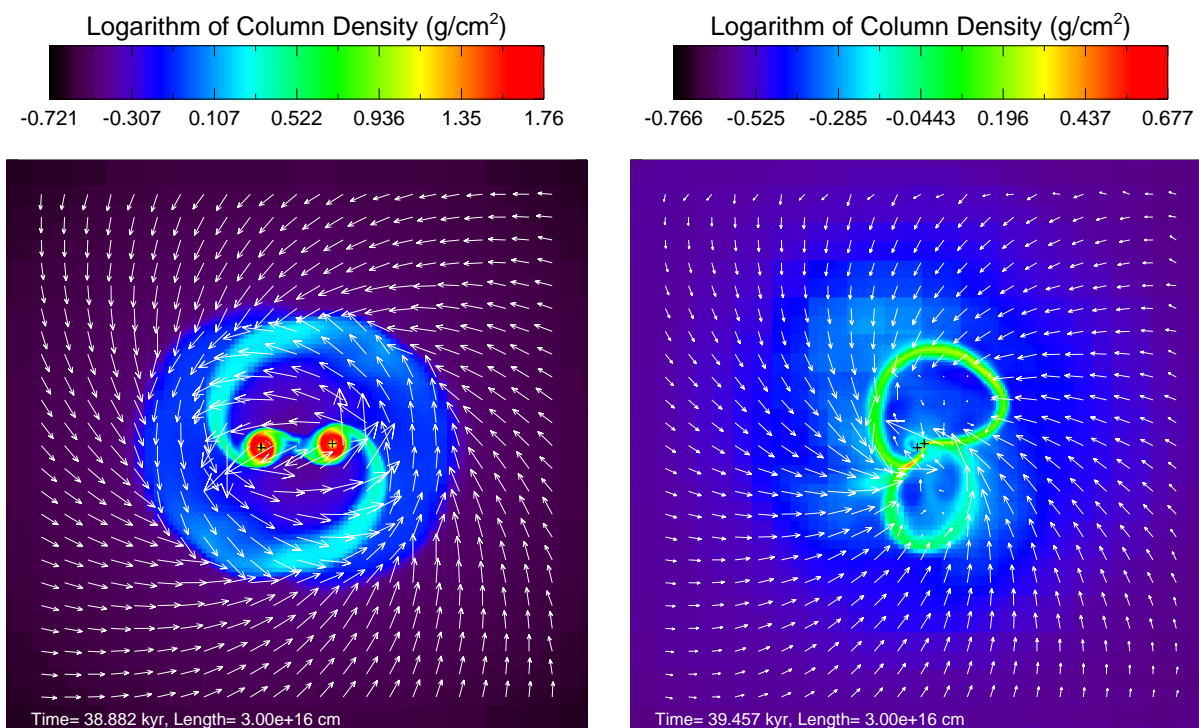


Fig. 1.— Distribution of the logarithm of the column density Σ (in $g \cdot cm^{-2}$) along z -direction and velocity field on the equatorial plane. Both the HD (left panel) and $\lambda = 2$ (right panel) case are at $t \approx 39$ kyr. The well-defined circumstellar and circumbinary disks in the former are replaced by two magnetically dominated lobes in the latter. The binary stars are marked by crosses.

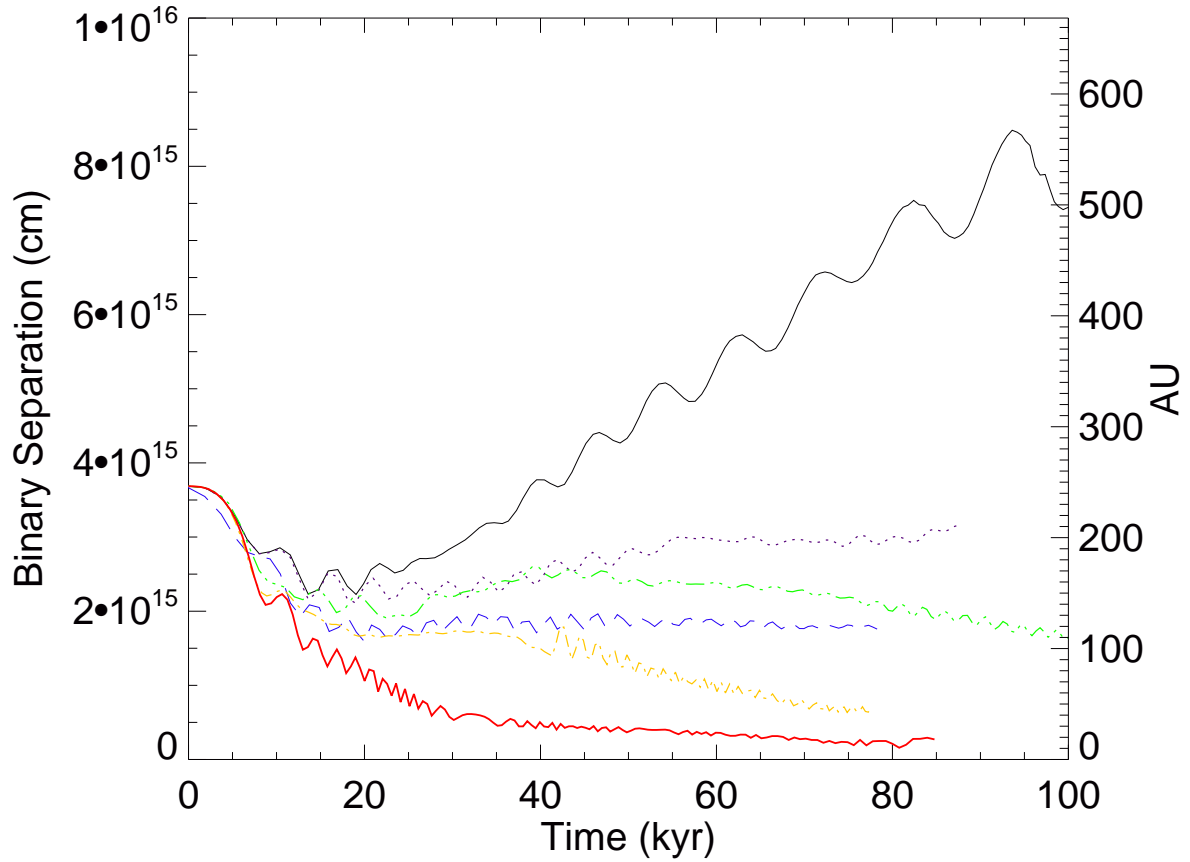


Fig. 2.— Evolution of binary separation with time for HD (black solid), $\lambda = 32$ (purple dotted), $\lambda = 16$ (blue long-dashed), $\lambda = 8$ (green dash-dot-dot-dotted), $\lambda = 4$ (yellow dash-dotted), and $\lambda = 2$ (red thick solid) cases. Note the large difference between the HD and the realistically magnetized ($\lambda = 2$ and perhaps 4) cases.

orbital angular momentum and total mass of the protobinary. The scaling can be obtained as follows. We assume that the gas in our singular isothermal envelope accretes shell by shell onto the binary. The total mass $M(r)$ and total angular momentum $L(r)$ for a sphere of radius r are given, respectively, by Eq. (2) and

$$L(r) = \frac{Ac_s^2 v_0}{3G} r^2. \quad (7)$$

If all of the mass and angular momentum of the material within the sphere are accreted onto the binary, then the orbital angular momentum L_b and binary mass M_b must be related through

$$L_b(M_b) = \frac{2Gv_0}{3Ac_s^2} M_b. \quad (8)$$

This relation is shown as the dashed line (scaled down by a factor of ~ 1.5) in Fig. 3, together with the angular momentum-mass (or L_b - M_b) relations obtained in all of our simulations. Again, the HD case is particularly noteworthy. Its $L_b - M_b$ relation closely matches the analytical prediction from eq. (8), except for a correction factor of ~ 1.5 . The correction is to be expected because the mass and orbital angular momentum of the protobinary at any given time does not come from a region of perfectly spherical shape (assumed in deriving the above equation). More slowly rotating material near the rotation axis can collapse more quickly onto the binary than that near the equator, lowering the actual angular momentum of the binary relative to its mass. In any case, the broad agreement between the numerical result on the L_b - M_b relation and the analytical expectation lends further credence to the correctness of the hydro simulation.

3.1.2. Magnetic Effect on Protobinary Orbit

Fig. 2 shows a general trend that the binary separation decreases with increasing magnetic field strength. The difference is especially striking at late times, when the separation increases with time for the HD case but stays roughly constant or decreases for the magnetized cases. By the time $t \approx 80$ kyr, the protobinary separation in the HD case reaches ~ 500 AU, which is much larger than that in the $\lambda = 4$ (~ 50 AU) and $\lambda = 2$ (~ 10 AU) case. There is little doubt that a realistic magnetic field (corresponding to a dimensionless mass-to-flux ratio of a few, see Troland & Crutcher 2008 and discussion in § 1) can shrink the protobinary orbit by a large factor.

The reduction in binary separation is related to a decrease in the orbital angular momentum of the system. This is shown explicitly in Fig. 3. There is a general trend for the orbital angular momentum to decrease with increasing magnetic field strength. When the

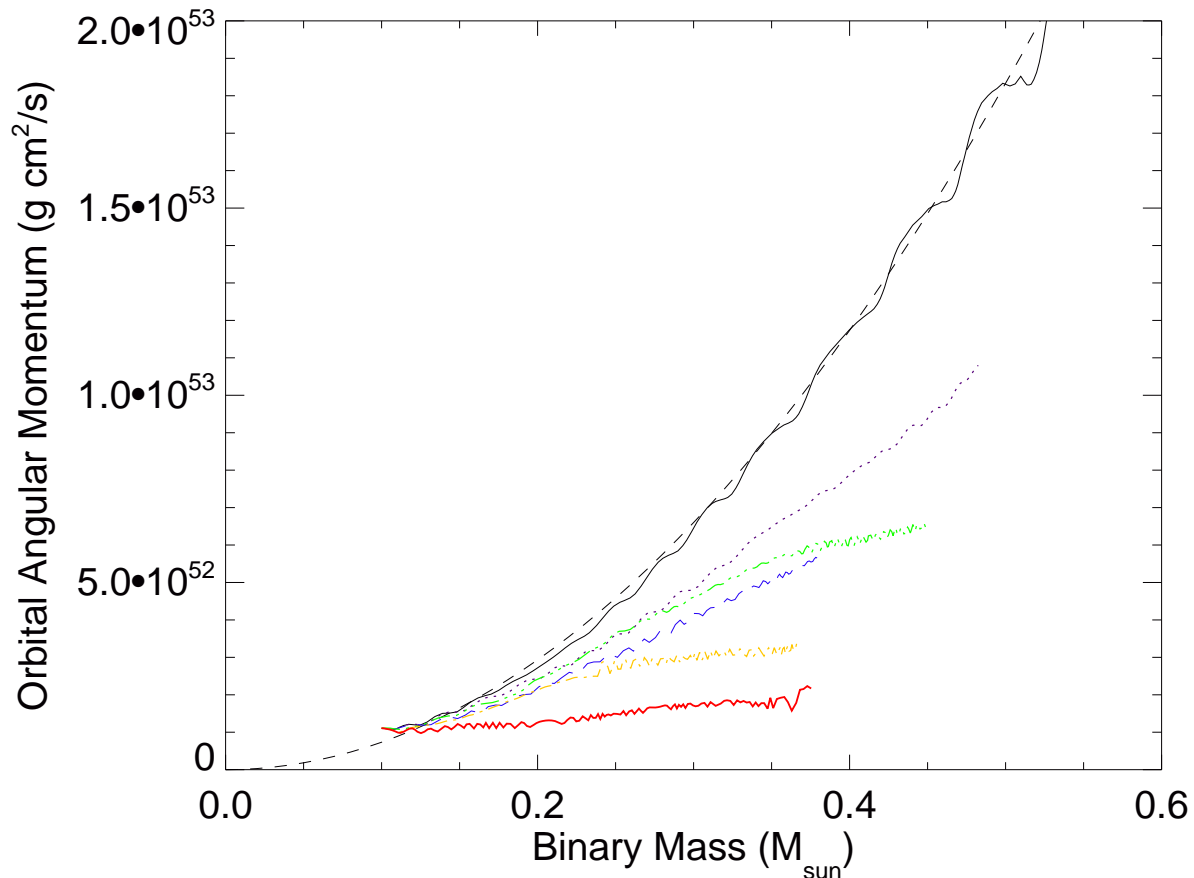


Fig. 3.— The relation between the orbital angular momentum and total mass of the proto-binary. The dash line is the the analytical prediction from Eq. 8 (reduced by a correction factor of ~ 1.5). The different curves are: HD (black solid), $\lambda = 32$ (purple dotted), $\lambda = 16$ (blue long-dashed), $\lambda = 8$ (green dash-dot-dot-dotted), $\lambda = 4$ (yellow dash-dotted), and $\lambda = 2$ (red thick solid).

mass of the stellar seeds quadruples from 0.1 to $\sim 0.4 M_{\odot}$, the orbit angular momentum in the HD case increases by more than an order of magnitude, whereas that in the strongly magnetized $\lambda = 2$ case increases by merely a factor of 2. In the latter case, there is a large amount of mass added to the protobinary but relatively little angular momentum. Since the binary separation a is sensitive to the orbital angular momentum L_b (i.e., $a \propto L_b^2$ for a fixed binary mass M_b), even a relatively modest change in the angular momentum would lead to a significant change in the separation.

We conclude from Figs. 3 and 2 that the main magnetic effect on the protobinary evolution is to reduce its orbital angular momentum compared to the non-magnetic case, which in turn leads to a tighter orbit. This result may appear puzzling at the first sight, because the magnetic forces do not act directly on the binary seeds. However, they do act on the material to be accreted by the seeds. By changing the angular momentum of such material, the magnetic field can greatly affect, perhaps even control, the orbital evolution of the protobinary. In the next subsection, we explore in some detail the mechanism through which the magnetic field shrinks the protobinary orbit.

3.2. Magnetic Braking and Angular Momentum Removal from Protobinary Accretion Flow

It is well-known that magnetic fields interact strongly with fluid rotation, through magnetic braking. If the infalling material has a large fraction of its angular momentum removed prior to its arrival at the binary seeds, it would add mass but relatively little angular momentum to the protobinary system. As a result, the binary separation would increase less rapidly with time compared to the hydro case; it may even decrease with time if the magnetic braking is strong enough.

The presence of magnetic braking can be seen directly from Fig. 4, where we plot the field lines at the representative time $t \approx 39$ kyr for the $\lambda = 2$ case. The initially straight field lines are twisted by the fluid rotation into helical shape, especially in the polar regions. The magnetic tension force associated with the twist acts back on the fluid, braking its rotation.

To quantify the strength of the magnetic braking, let us consider a finite volume V with surface S . Inside this volume, the total magnetic torque relative to the origin (from which a radius vector \mathbf{r} is defined) is

$$\mathbf{N}_m = \frac{1}{4\pi} \int [\mathbf{r} \times ((\nabla \times \mathbf{B}) \times \mathbf{B})] dV, \quad (9)$$

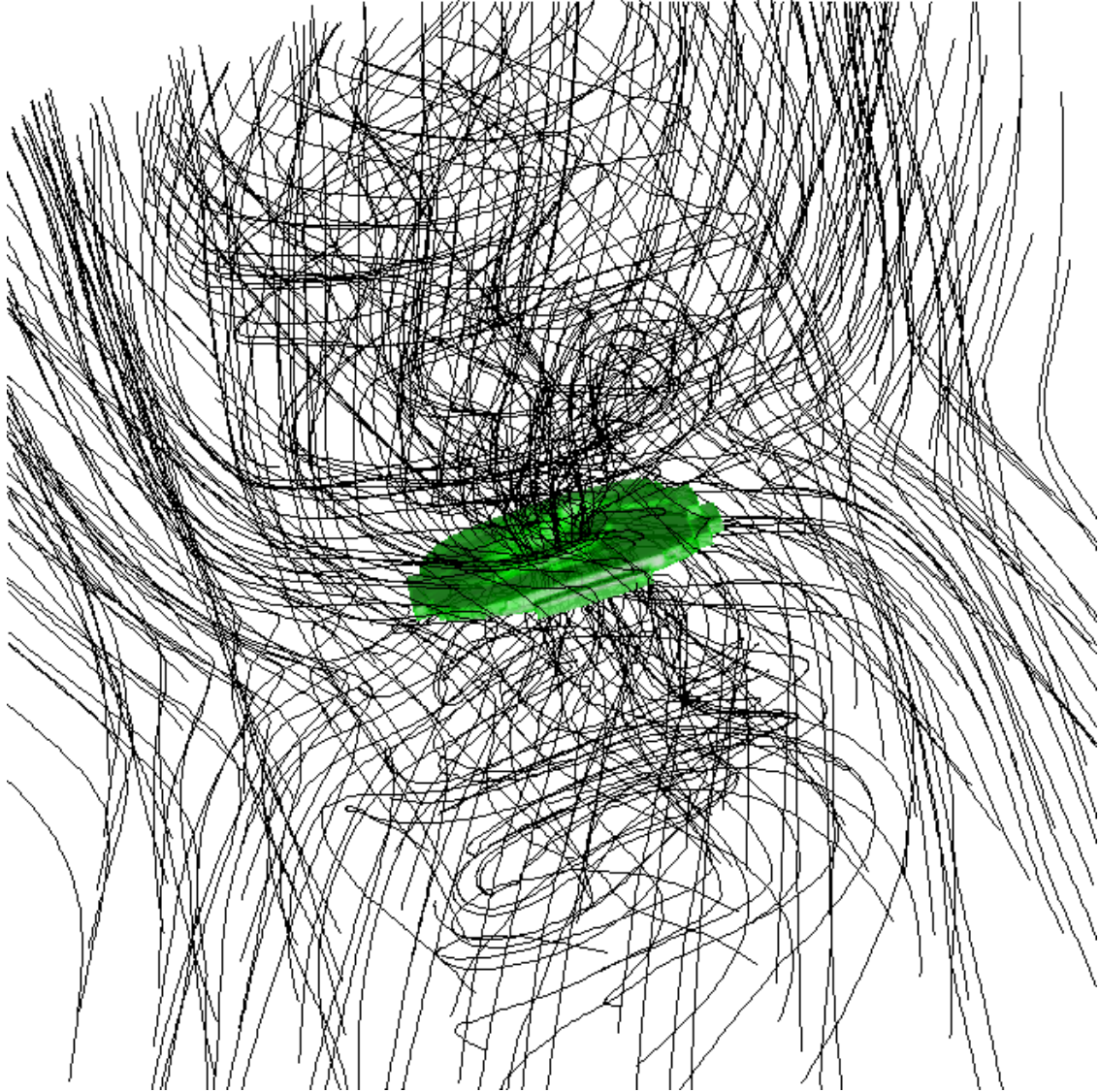


Fig. 4.— 3D view of the magnetic field lines and an iso-density surface in the inner part of the protobinary accretion flow at the representative time $t \approx 39$ kyr, showing the field twisting that is the smoking gun of magnetic braking. The plotted region has a dimension of 5×10^{15} cm.

where the integration is over the volume V . Typically, the magnetic torque comes mainly from the magnetic tension rather than pressure force. The dominant magnetic tension term can be simplified to a surface integral (Matsumoto & Tomisaka 2004)

$$\mathbf{N}_t = \frac{1}{4\pi} \int (\mathbf{r} \times \mathbf{B})(\mathbf{B} \cdot d\mathbf{S}), \quad (10)$$

over the surface S of the volume. This volume-integrated magnetic torque is to be compared with the rate of angular momentum advected into the volume through fluid motion,

$$\mathbf{N}_a = - \int \rho(\mathbf{r} \times \mathbf{v})(\mathbf{v} \cdot d\mathbf{S}), \quad (11)$$

which will be referred to as the advective torque below.

Since the initial angular momentum of the protobinary envelope is along the z -axis, we will be mainly concerned with the z -component of the magnetic and advective torque,

$$N_{t,z} = \frac{1}{4\pi} \int (xB_y - yB_x)(\mathbf{B} \cdot d\mathbf{S}) \quad (12)$$

and

$$N_{a,z} = - \int \rho(xv_y - yv_x)(\mathbf{v} \cdot d\mathbf{S}), \quad (13)$$

which can change the z -component of the angular momentum L_z within the volume V .

As an example, we show in Fig. 5 the distributions of the magnetic and advective torques $N_{t,z}$ and $N_{a,z}$ for cubic boxes of different sizes that are centered at the origin, at the representative time $t \approx 39$ kyr for the $\lambda = 2$ case. As expected, the volume-integrated magnetic torque is negative for boxes of most sizes; it removes angular momentum from the material inside the boxes through magnetic braking. At the time shown, the braking torque is particularly large outside $\sim 10^{16}$ cm from the origin, reaching absolute values of order 10^{41} g cm²s⁻² or larger. To appreciate how large this torque is, we note that the orbital angular momentum of the protobinary in the hydro case is $\sim 4.4 \times 10^{52}$ g cm²s⁻¹ around the same time. This angular momentum would be removed by the above magnetic torque on a time scale of 13 kyr, much shorter than the envelope collapse time. Given the magnitude of the magnetic torque, it is not surprising that the orbital angular momentum (and thus the separation) of the protobinary can be reduced significantly.

The magnetic torque changes with time, however. At the time shown in Fig. 5, the magnetic torque overwhelms the advective torque for boxes of most sizes, leading to a net decrease of the angular momentum with time for the material in these boxes. This may not

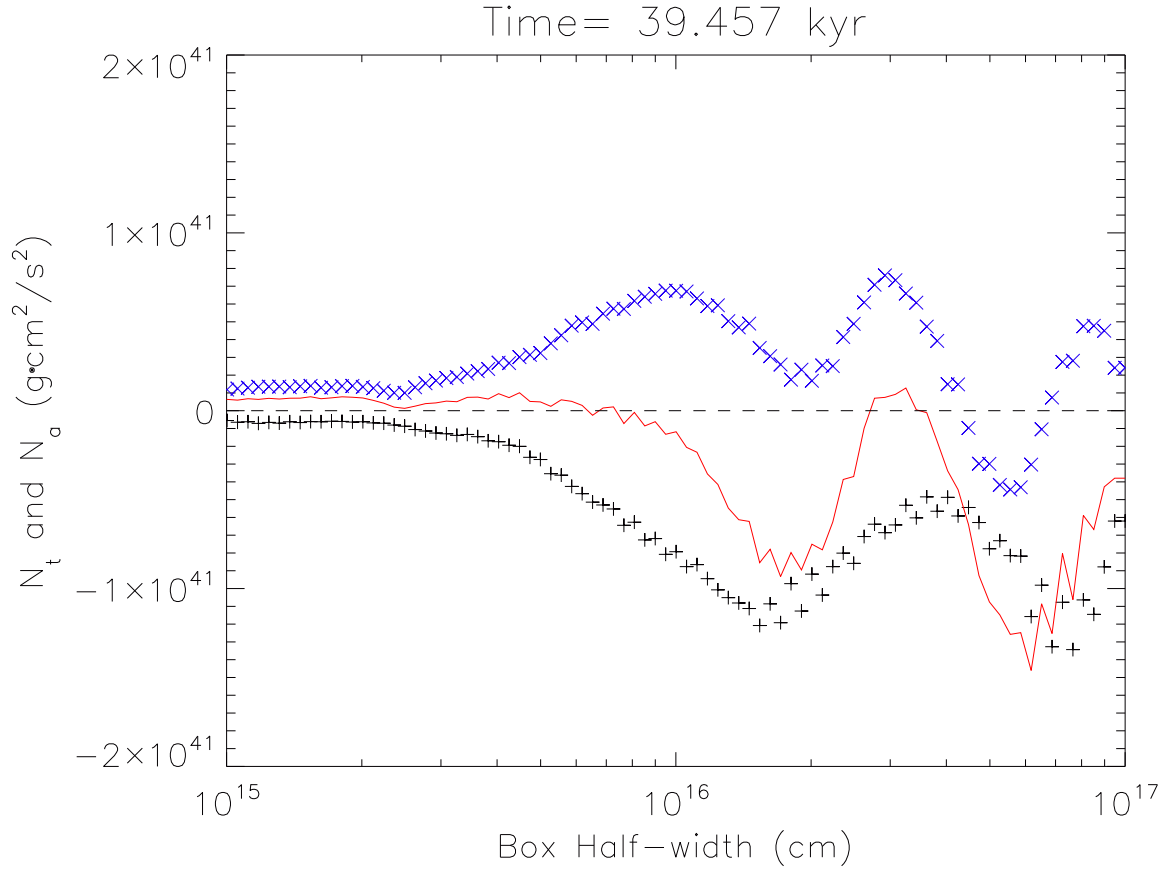


Fig. 5.— The magnetic (black ‘+’) and advective (blue ‘x’) torque and the sum of the two (red) for cubic boxes of different half-width b for the $\lambda = 2$ case, at a representative time $t \approx 39$ kyr. A positive torque increases the angular momentum within a volume whereas a negative one decreases it.

happen at other times. To evaluate the accumulative effects of the magnetic and advective torque over time, we define for each box of half width b

$$L_{t,z}(b, t) = \int_0^t N_{t,z}(b, t') dt' \quad (14)$$

and

$$L_{a,z}(b, t) = \int_0^t N_{a,z}(b, t') dt' \quad (15)$$

which are the amount of the z -component of the angular momentum inside the box changed by the magnetic and convective torque, respectively, up to time t . These two quantities are to be compared with the actual change of the angular momentum inside each box between time t and $t = 0$,

$$\Delta L_z(b, t) = L_z(b, t) - L_z(b, t = 0). \quad (16)$$

Barring a significant gravitational torque, one expects $\Delta L_z(b, t)$ to be close to $L_{a,z}(b, t)$ in the hydro case, because fluid advection should be the main channel for angular momentum change. This is indeed the case, as illustrated in panel (a) of Fig. 6, where both $\Delta L_z(b, t)$ and $L_{a,z}(b, t)$ are plotted as a function of the box size b at the representative time $t \approx 39$ kyr. The change in angular momentum $\Delta L_z(b, t)$ does follow closely the advected angular momentum for boxes of sizes larger than $\sim 10^{16}$ cm. For boxes of smaller sizes, there is significantly more angular momentum advected into a box than the actual angular momentum change in it, indicating that a good fraction of the angular momentum advected into the box is transported back out, presumably by the gravitational torques associated with the spiral arms that are visible in the left panel of Fig. 1. The gravitational torques may also be responsible for the small excess of $L_{a,z}(b, t)$ over $\Delta L_z(b, t)$ for the larger boxes.

The situation is very different in the presence of a relatively strong magnetic field, as shown in panel (b) of Fig. 6. Plotted are $L_{t,z}(b, t)$, $L_{a,z}(b, t)$, and $L_{t,z}(b, t) + L_{a,z}(b, t)$ together with $\Delta L_z(b, t)$ as a function of box size at $t \approx 39$ kyr for the $\lambda = 2$ case. The total change of the angular momentum due to the magnetic and advective torque acting on the boundary of a box, $L_{t,z}(b, t) + L_{a,z}(b, t)$, is very close to the actual change in angular momentum inside the box, $\Delta L_z(b, t)$, indicating that any additional torques (such as gravitational torques), if present, play a relatively minor role in angular momentum transport. This is not surprising, because the prominent spiral arms of the hydro case are disrupted by the magnetic field completely. More importantly, the sum $L_{t,z}(b, t) + L_{a,z}(b, t)$ has a magnitude much smaller than $|L_{t,z}(b, t)|$ and $|L_{a,z}(b, t)|$ individually, which means that most of the angular momentum advected into a box is removed by the magnetic braking, leaving little net angular momentum change in it. This is unequivocal evidence that the magnetic braking in the $\lambda = 2$ case

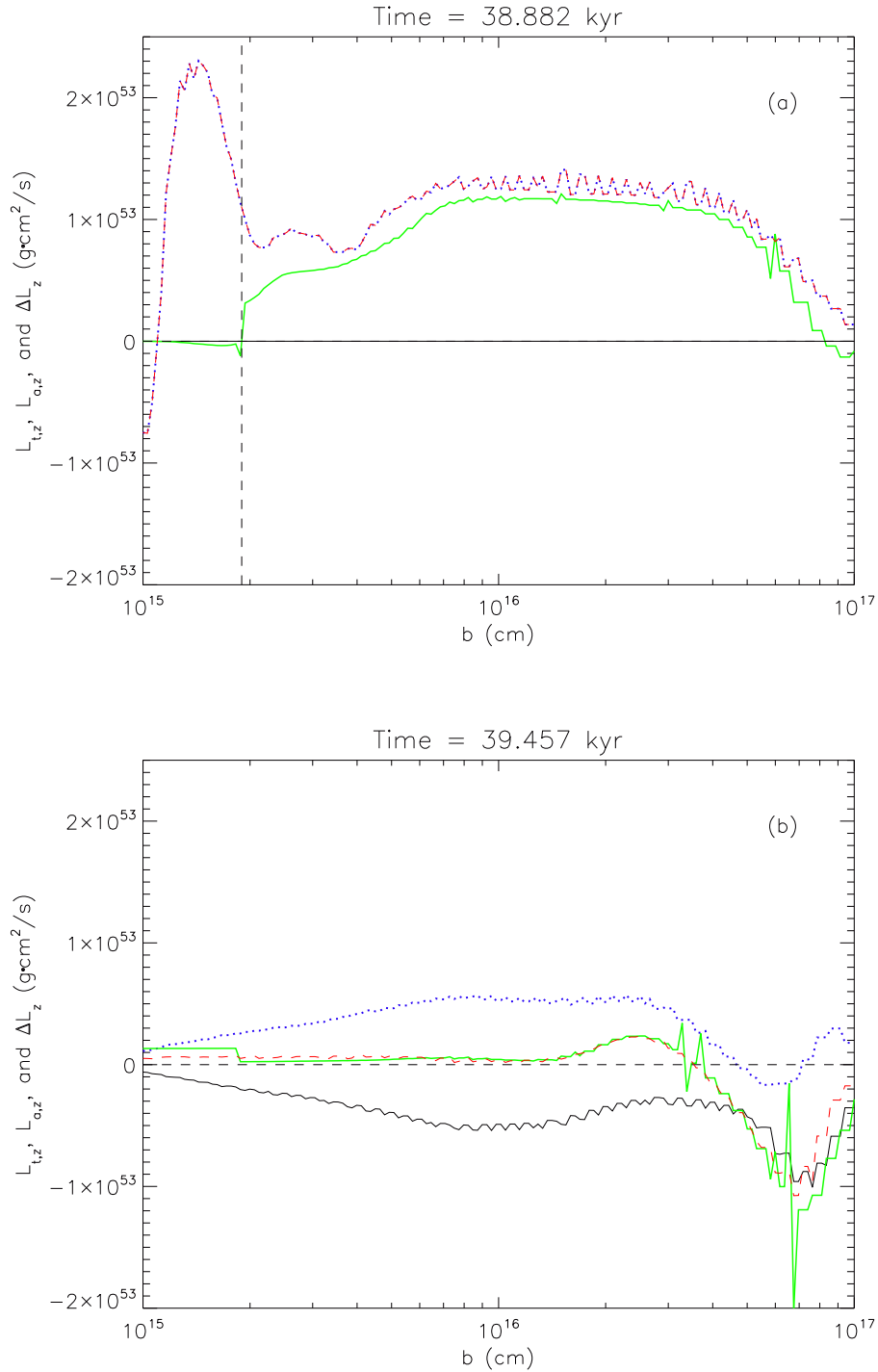


Fig. 6.— The integrated magnetic and advective torques $L_{t,z}$ (black solid), $L_{a,z}$ (blue dotted), and their sum $L_{t,z} + L_{a,z}$ (red dashed) together with the actual angular momentum change ΔL (green thick solid) for cubic boxes of different half-width b . The HD case is shown in panel (a) with zero $L_{t,z}$ and the $\lambda = 2$ case is shown in panel (b), both at a similar time $t \approx 39$ kyr. The vertical dashed line in panel (a) indicates the approximate position of the sink particles, whereas in panel (b) such particle position lies below 10^{15} cm.

controls the angular momentum evolution of the protostellar accretion flow, which in turn shapes the orbit of the protobinary.

The effect of magnetic braking is even stronger than indicated by panel (b) of Fig. 6. This is because $L_{a,z}(b, t)$ is the net angular momentum advected into a box, i.e., the sum of the positive angular momentum advected into the box $L_{a,z}^+(b, t)$ and the negative angular momentum advected out of the box $L_{a,z}^-(b, t)$. In the $\lambda = 2$ case, the magnetic braking drives an outflow, which produces a negative angular momentum $L_{a,z}^-(b, t)$ that is not much smaller in magnitude than $L_{a,z}^+(b, t)$. In other words, the angular momentum advected by infall into a box is larger than that shown in Fig. 6, and most of this larger angular momentum is removed by both the magnetic braking itself and the braking-induced outflow.

To illustrate the effect of magnetic braking more visually, we plot in Fig. 7 the distribution of specific angular momentum on the equatorial plane for the hydro and $\lambda = 2$ case at the representative time $t \approx 39$ kyr. It is clear that, for the hydro case, the specific angular momentum is roughly constant within a dimensionless radius of ~ 0.05 (or $\sim 2.5 \times 10^{16}$ cm), indicating that the collapsing material has a more or less conserved angular momentum before it is accreted by the protobinary. The relatively large specific angular momentum of the accreted material is what drives the binary separation to increase. In the $\lambda = 2$ case, the specific angular momentum of the material to be accreted is much smaller; it is reduced by twisted field lines (see Fig. 4) as the material falls toward the binary. It is the accretion of the severely braked, low angular momentum material that drives the protobinary closer with time.

3.3. Circumstellar and Circumbinary Structures

We have already seen from Fig. 1 that a realistic magnetic field of $\lambda = 2$ changes the circumstellar and circumbinary structures of the HD case greatly: the prominent features of the HD case, two well-defined circumbinary disks and a circumbinary disk with two prominent spiral arms, are replaced by two low density lobes, which are filled with the magnetic flux decoupled from the matter that has been accreted onto the binary, i.e., the DEMS (Zhao et al. 2011; see also Seifried et al. 2011; Joos et al. 2012; Krasnopolsky et al. 2012). These strongly magnetized structures present an obstacle to mass accretion onto the protobinary. Although the DEMS tend to be less prominent for weaker magnetic fields, they still dominate the face-on view of the $\lambda = 4$ and 8 cases, especially at late times. An implication is that, for protostellar envelopes magnetized to a realistic level (with $\lambda \sim$ a few), the protobinary mass accretion does not follow the traditional path: from the envelope to a circumbinary disk to circumstellar disks to individual stars. Rather, the envelope material

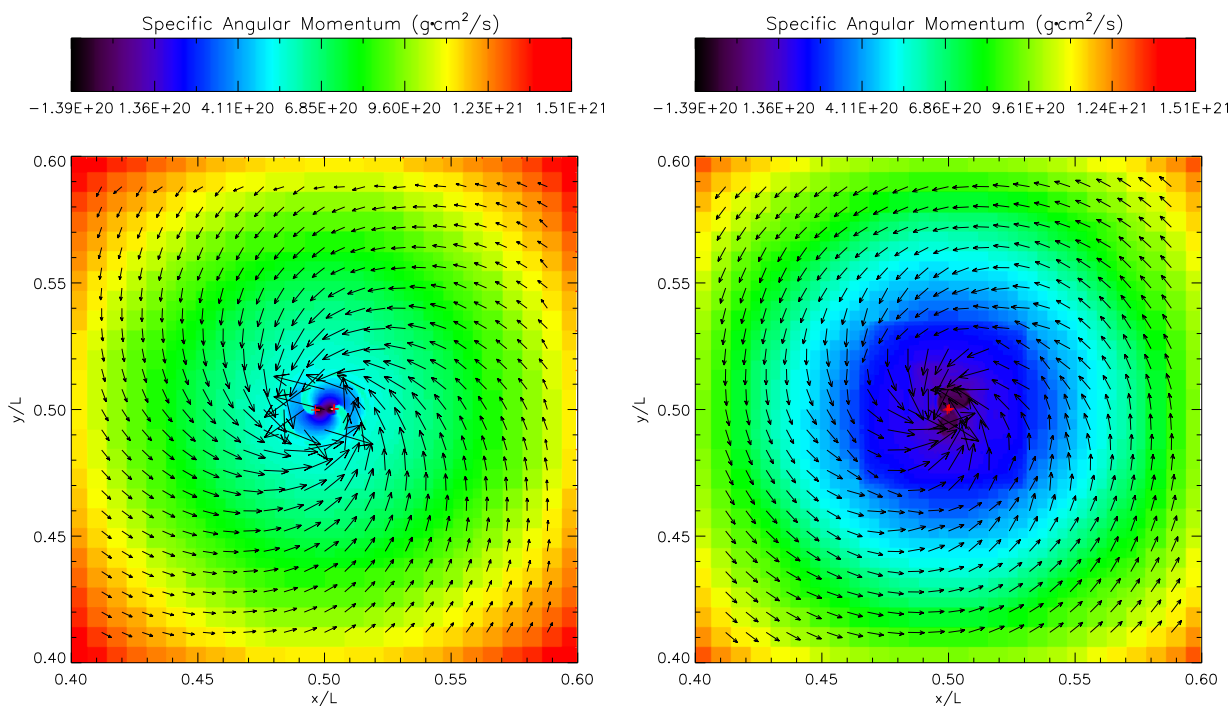


Fig. 7.— Snapshot of the gas specific angular momentum (in $g \cdot cm^2 \cdot s^{-1}$ with logarithm scale) on the equatorial plane of the inner accretion flow for the HD case (left panel) and the $\lambda = 2$ case (right panel) at $t \approx 39$ kyr, showing the strong braking of the material to be accreted by the protobinary in the magnetized case compared to the HD case. The arrows are velocity vectors, and the crosses mark stars. Only the central region of 10^{17} cm on each side is plotted.

collapses directly close to the stars typically, and be accreted along azimuthal directions not occupied by the DEMS.

Another magnetic effect on the circumbinary environment is illustrated in Fig. 8, where we display both the edge-on and face-on view of the $\lambda = 2$ case at a relatively early time $t = 18$ kyr. The edge-on view shows that the protobinary is surrounded by two large, mostly expanding, regions (one each above and below the equator) that are absent in the HD case. Their dynamics are dominated by the rotationally twisted magnetic fields (see Fig. 4). It is in these regions that most of the angular momentum extracted magnetically from the material that falls into the stars is stored. Such bipolar expanding regions are seen in many magnetized core collapse simulations (for an early example, see Tomisaka 1998). They block the protobinary accretion over most of the solid angle, and force the accretion to occur mainly through a flattened, equatorial structure — a circumbinary pseudodisk (Galli & Shu 1993).

The pseudodisk is also clearly visible in the face-on view of the system in the right panel of Fig. 8, as a nearly circular region of enhanced column density. Unlike the circumbinary disk in the HD case (see the left panel of Fig. 1), the pseudodisk is not rotationally supported. It falls supersonically inward, and the infall can be seen in the velocity fields shown in Fig. 8. Another difference is that the circumbinary pseudodisk does not have prominent spiral arms. This is not surprising, because the pseudodisk is strongly magnetized, which makes gas compression more difficult. The rapid infall also leaves little time for the spirals to develop. The lack of spiral arms is consistent with our earlier result that the angular momentum transport in the $\lambda = 2$ case is dominated by magnetic braking rather than gravitational torque.

3.4. Protobinary Mass Growth

Despite the differences in the morphology and dynamics of the circumbinary environment with and without a magnetic field, the stars grow at remarkably similar rates in all cases (of order $\sim 10^{-6} M_{\odot}/\text{yr}$). This is shown in Fig. 9, where the mass of each component of the protobinary is plotted as a function of time, for different degrees of magnetization. The reason for the similarity is that the mass accretion rate is determined mainly by the dynamics on the envelope scale: the material collapsing down from the envelope will find a way to the stars sooner or later, irrespective of the details of the circumbinary environment. In the HD or weakly magnetized cases, there is more material parked in the circumstellar and circumbinary disks, making the mass accreting rate onto the stars lower. However, this effect is smaller than that from the retardation of envelope collapse by magnetic tension in

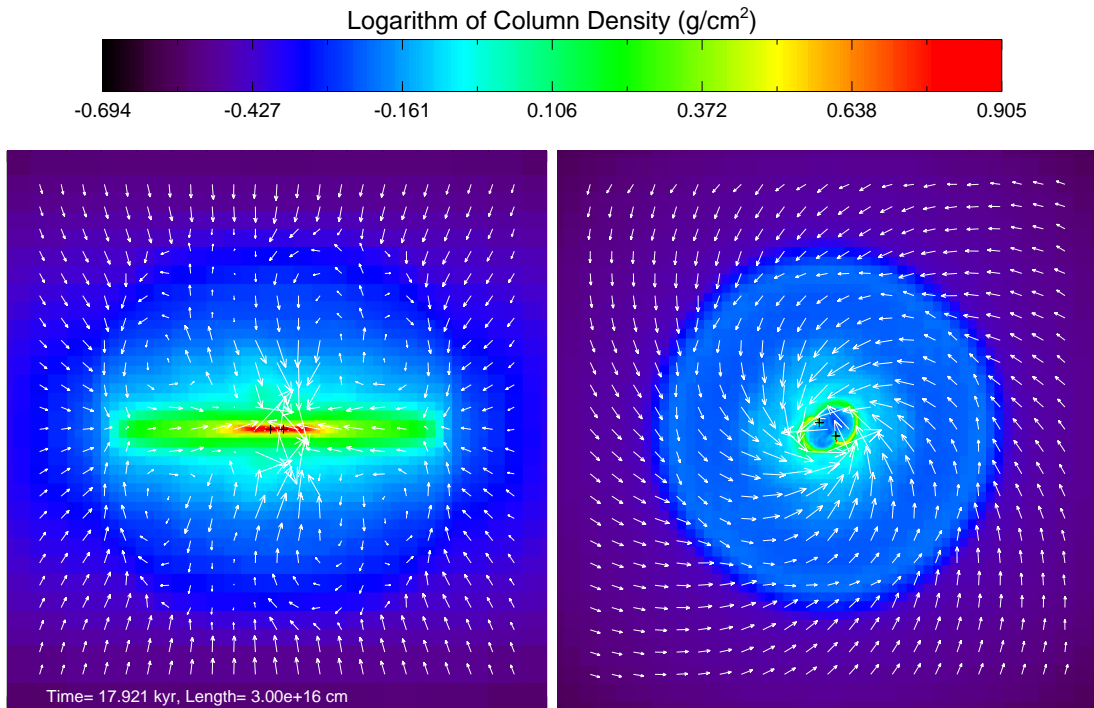


Fig. 8.— Left panel: edge-on view of the column density in the $\lambda = 2$ case at $t = 18$ kyr, showing two slowly expanding polar regions sandwiching an infalling, circumbinary pseudodisk in the equatorial region. Right panel: face-on view of the same structure, showing that the circumbinary pseudodisk is not rotationally supported; it collapses rapidly.

the stronger field cases. As a result, the protostellar mass accretion rate is somewhat lower in the stronger field cases, although not by a large factor.

It is reassuring that the masses of the two initially equal-mass components stay nearly the same for all cases, despite the fact that the inner protobinary accretion flow can become rather disordered at times, especially for strongly magnetized cases. The magnetic field does not appear to change much the rate of mass accretion by one component relative to the other, although the situation is drastically different for initially unequal mass protobinaries, as we demonstrate next.

4. Magnetic Braking and Mass Ratio of Unequal-Mass Protobinaries

The vast majority of low (Sun-like) mass binaries are unequal-mass systems (Duquennoy & Mayor 1991; Raghavan et al. 2010). The mass ratio, defined as $q = M_2/M_1$ where M_1 and M_2 are the mass of the primary and secondary respectively, is one of the fundamental parameters that characterize the binaries. Its observed distribution provides important constraints on binary formation and evolution (see discussion in § 5).

The mass ratio q of protobinaries is expected to be affected by magnetic braking. This is because the change of q depends on the specific angular momentum of the circumbinary material to be accreted relative to that of the binary. It is well known that high angular momentum material tends to accrete preferentially onto the less-massive secondary, which has a higher specific angular momentum than the primary, driving the mass ratio toward unity (Bate & Bonnell 1997; Bate et al. 2002). As we have seen above, magnetic braking can remove the angular momentum of the circumbinary material efficiently. It is expected to weaken the tendency for preferential accretion onto the secondary. We show that it is indeed the case in Fig. 10.

Shown in Fig. 10 are the mass ratios as a function of time for three cases $\lambda = \infty$ (HD), 16 and 2. The initial conditions are the same as those for the equal-mass cases discussed in § 3, except that the mass and angular momentum inside the radius r_h of the power-law envelope are given to a binary system of mass ratio $q = 0.25$ rather than $q = 1$. The mass ratio increases with time in the HD case, in agreement with previous results. As expected, the magnetic field slows down the increase in q compared to the HD case. Even a rather weak magnetic field of $\lambda = 16$ has an appreciable effect on the mass ratio evolution. For the more realistic value of $\lambda = 2$, the primary accretes much faster than the secondary, by a factor of 3-4, so that the mass ratio remains roughly constant. The large contrast between the HD and $\lambda = 2$ case leaves little doubt that magnetic braking is an important

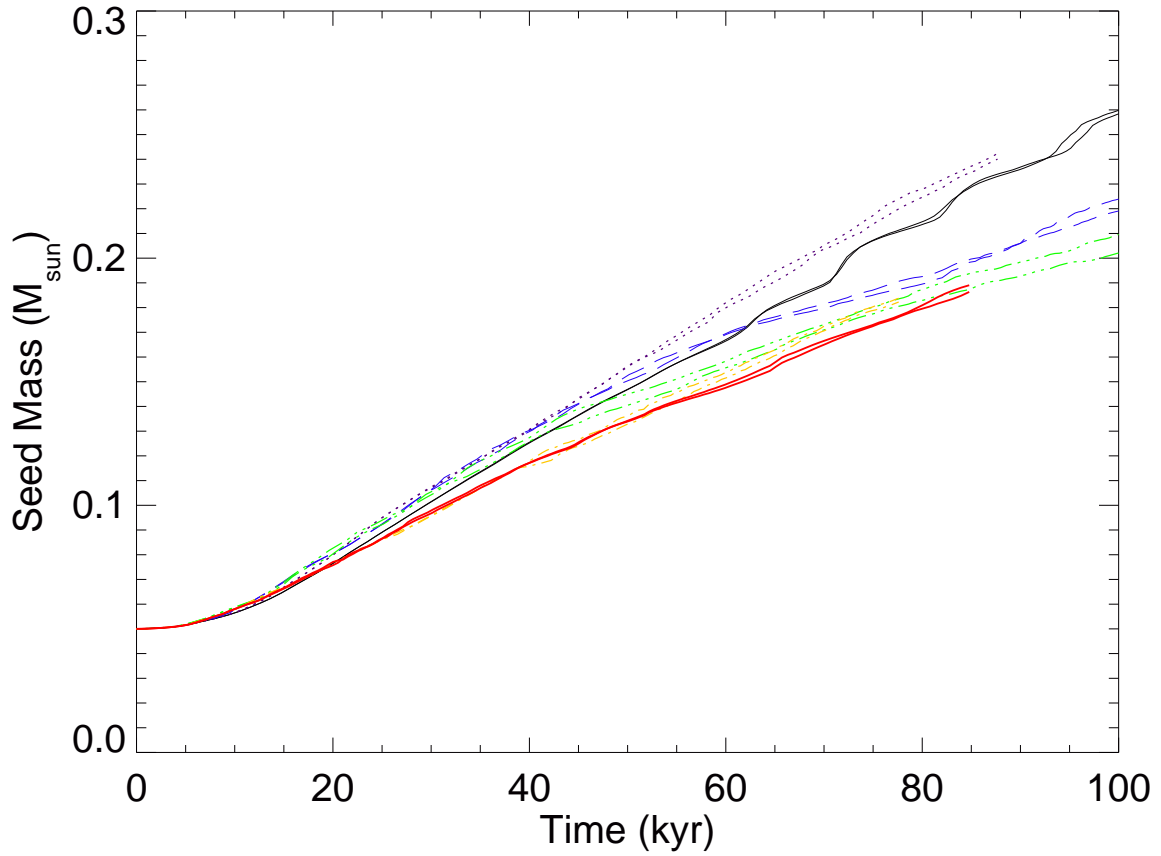


Fig. 9.— Stellar mass (in solar units) growth of the initially equal-mass binary system for HD (black solid), $\lambda = 32$ (purple dotted), $\lambda = 16$ (blue long-dashed), $\lambda = 8$ (green dash-dot-dot), $\lambda = 4$ (yellow dash-dot), and $\lambda = 2$ (red thick solid) cases. Note that, in all cases, the two stars stay roughly equal-mass at all times.

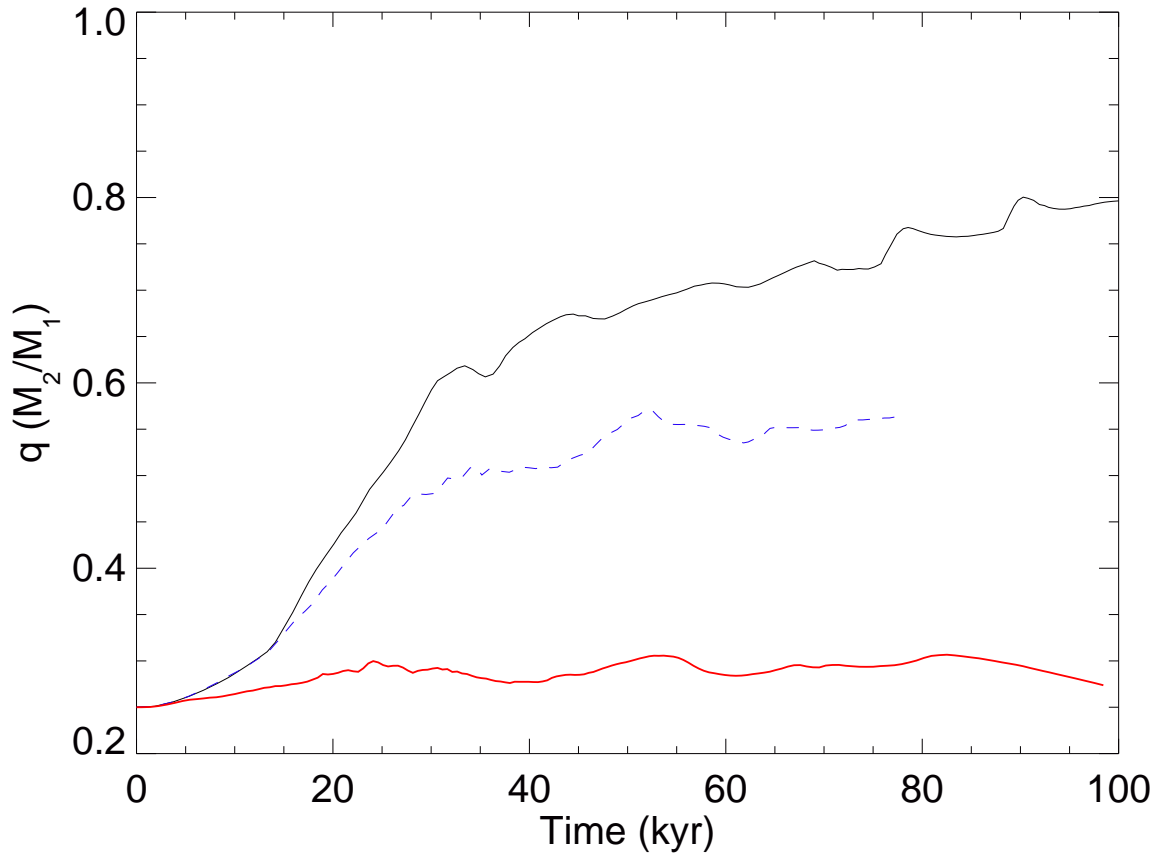


Fig. 10.— Evolution of the protobinary mass ratio q with time for envelopes that have different levels of magnetization, with $\lambda = \infty$ (HD, black solid), 16 (blue dashed), and 2 (red thick solid).

factor to consider in understanding the mass ratio distribution of binaries. We will leave a comprehensive exploration of this issue to a future investigation.

5. Summary and Discussion

We have carried out a set of idealized numerical experiments to demonstrate the effects of the magnetic field on protobinary evolution during the mass accretion phase. The protostellar envelope was idealized as a rotating, magnetized singular isothermal sphere. Its collapse onto a pre-existing pair of binary seeds was followed using an MHD version of the ENZO AMR hydro code that includes a sink particle treatment. We found that a magnetic field of the observed strength (corresponding to a dimensionless mass-to-flux ratio of a few) can remove, through magnetic braking, most of the angular momentum of the material that reaches the protobinary. The reduction in the angular momentum of the protobinary accretion flow has two important consequences: compared to the non-magnetic case, (1) the protobinary orbit becomes much tighter, and (2) the mass-ratio does not increase as fast with time for initially unequal mass systems. In addition, the magnetic field drastically changes the morphology and dynamics of the structures that surround the protobinary. It suppresses the formation of the familiar circumstellar and circumbinary disks in the non-magnetic case, as well as the spiral arms embedded in them. These structures are replaced by a bipolar magnetic-braking driven expanding regions, a dense, infalling, circumbinary pseudodisk in the equatorial region, and low-density, highly magnetized structures close to the protobinary that expand against the pseudodisk (the DEMS). We conclude that both the basic characteristics (such as mass ratio and separation) of the protobinaries and the environment in which binaries grow are strongly modified by a realistic magnetic field.

The magnetic braking-driven inward migration of protobinaries may have observable consequences. As mentioned in the introduction, the distribution of binary orbital separation during the earliest, Class 0 phase of star formation may be different from those at later times. In particular, there is tentative evidence for a “desert” free of Class 0 binaries with separation between $\sim 150 - 550$ AU (Maury et al. 2010; Enoch et al. 2011), which is not present in the Class I or later phases. If confirmed by future observations, this gap must be filled in by binaries from either outside the gap or interior to it. The magnetic braking is an efficient way of shrinking the protobinary orbit. It can in principle move some binaries born on wide orbits outside the gap into the gap. Indeed, Offner et al. (2009, 2010) found that most of the binaries in their cluster formation simulations were born with relatively wide separations, as a result of radiative feedback, which tends to suppress close binary formation through disk

fragmentation; the orbits of such wide binaries could be tightened by magnetic braking². A potential problem is that the braking may be so efficient during the protobinary mass accretion phase (when a massive, slowly rotating envelope is still present) that the binary separation would move quickly through the gap and pile up below the resolution of the current generation of millimeter/submillimeter interferometers ($\sim 50 - 100$ AU). If this is the case, one would expect to find an over-abundance of relatively close protobinaries with separation $\lesssim 100$ AU that may be uncovered by ALMA and JVLA. The same pileup at small separations would also occur if the binaries born on tight orbits interior to the gap are kept from expanding into the gap by magnetic braking.

The problem of potentially turning most wide binaries into close binaries is related to the magnetic braking catastrophe in disk formation (Galli et al. 2006). Both semi-analytic arguments and numerical simulations have shown that, in magnetized laminar dense cores of λ of a few, the formation of a rotationally supported disk is suppressed by magnetic braking in the ideal MHD limit (Allen et al. 2003; Galli et al. 2006; Price & Bate 2007; Mellon & Li 2008; Hennebelle & Fromang 2008; Seifried et al. 2011; Dapp & Basu 2011). The magnetic braking must be weakened somehow in order to form both large-scale disks and wide binaries. In the context of disk formation, there are several proposed mechanisms for weakening the magnetic braking, including the misalignment between the magnetic and rotation axes (Joos et al. 2012), turbulence (Santos-Lima et al. 2012; Seifried et al. 2012; Myers et al. 2012), and the depletion of the slowly rotating protostellar envelope that acts to brake the disk, either by outflow stripping (Mellon & Li 2008) or accretion (Machida et al. 2010). The last possibility is particularly intriguing, because it implies a rapid growth of the rotationally supported disk during the transition from the deeply embedded Class 0 phase to the more revealed Class I phase that can be observationally tested. Similarly, the depletion of the protobinary envelope and the associated weakening of magnetic braking may enable the separation of the protobinaries to grow quickly during the Class 0-Class I transition. If this is the case, the orbits of wide binaries may first shrink during the Class 0 phase due to efficient magnetic braking and then re-expand as the protobinary envelope depletes. This and other possibilities for protobinary migration should be testable with high-resolution millimeter/submillimeter interferometric observations, especially using ALMA and JVLA.

Our calculations demonstrated that magnetic braking is important for the evolution of not only the binary separation, but also the mass ratio q . Raghavan et al. (2010) found a

²Bate (2012) found that the binaries in his radiation hydro simulations of cluster formation have properties consistent with observations, indicating that magnetic effects are not needed. It would be interesting to quantify how a magnetic field of the observed strength modifies the properties of the binaries formed in a cluster environment.

roughly flat distribution for q between 0.2-0.95, with a valley below 0.2, and three spikes around 0.25, 0.35 and 1.0 (see the left panel of their Fig. 16). It is tempting to attribute the last spike at $q \sim 1$ to the preferential accretion of high specific angular momentum material onto the lower-mass component found in hydrodynamical simulations (Bate & Bonnell 1997; Bate et al. 2002). However, the spike around $q \sim 1$ is just one of the three spikes in Raghavan et al.’s data, and it does not show up in the sample of Duquennoy & Mayor (1991) at all (see their Fig. 10). In any case, there are many more systems with mass ratio q well below unity than close to unity. A mechanism must be found to prevent the majority of the low-mass ratio protobinaries from becoming equal-mass systems. The magnetic braking highlighted in this paper is one such mechanism. It is a key factor to consider in understanding binary formation and evolution in dense cores that are observed to be significantly magnetized.

We thank P. Arras, S. Offner, K. Kratter, C. Matzner, and A. Maury for useful discussion and P. Wang for advice on the ENZO code. This work is supported in part by NASA NNX10AH30G.

REFERENCES

- Allen, A., Li, Z. -Y., & Shu, F. H. 2003, *ApJ*, 599, 363
- Artymowicz P. 1983, *Acta Astron*, 33, 223
- Bate, M. R., Bonnell, I. A., & Bromm, V. 2002, *MNRAS*, 336, 705
- Bate, M. R., & Bonnell, I. A. 1997, *MNRAS*, 285, 33
- Bate, M. R. 2000, *MNRAS*, 314, 33
- Bate, M. R. 2012, *MNRAS*, 123
- Boss, A., & Bodenheimer, P. 1979, *ApJ*, 234, 289
- Bryan, G. L., & Norman, M. L. 1997, *astro-ph/9710187*
- Connelley, M. S., Reipurth, B., & Tokunaga, A. T. 2008, *AJ*, 135, 2526
- Dapp, W. B., & Basu, S. 2011, *A&A*, 532, 2
- Dedner, A., Kemm, F. Kröner, D., Munz, C. -D., Schnitzer, T., & Wesenberg, M. 2002, *Journal of Computational Physics*, 175, 645

- Duchêne, G., Bouvier, J., Bontemps, S., André, P., & Motte, F. 2004, *A&A*, 427, 651
- Duchêne, G., Bontemps, S., Bouvier, J., André, P., Djupvik, A. A., & Ghez, A. M. 2007, *A&A*, 476, 229
- Duquennoy, A., & Mayor, M. 1991, *A&A*, 248, 485
- Enoch, M. L., Corder, S., Duchêne, G., Bock, D. C., Bolatto, A. D., Culverhouse, T. L., Kwon, W., Lamb, J. W., Leitch, E. M., Marrone, D. P., Muchovej, S. J., Pérez, L. M., Scott, S. L., Teuben, P. J., Wright, M. C. H., & Zauderer, B. A. 2011, *ApJS*, 195, 21
- Fischer, D. & Marcy, G. 1992, *ApJ*, 396, 178
- Galli, D., Lizano, S., Shu, F. H., & Allen, A. 2006, *ApJ*, 647, 374
- Galli, D., & Shu, F. H. 1993, *ApJ*, 417, 243
- Goodman, A. A., Benson, P., Fuller, G. A., & Myers, P. C. 1993, *ApJ*, 406, 528
- Goodwin, S. P., & Kroupa, P. 2005, *A&A*, 439, 565
- Hanawa, T., Ochi, Y. & Ando, K. 2010, *ApJ*, 708, 485
- Hennebelle, P., & Fromang, S. 2008, *A&A*, 477, 9
- Hennebelle, P., & Teyssier, R. 2008, *A&A*, 477, 25
- Janson, M., Hormuth, F., Bergfors, C., Brandner, W., Hippler, S., Daemgen, S., Kudryavtseva, N., Schmalzl, E., Schnupp, C., & Henning, T. 2012, arXiv:1205.4718
- Joos, M., Hennebelle, P., & Ciardi, A., *A&A*, 543, 128
- Krasnopolsky, R., Li, Z.-Y., Shang, H. & Zhao, B. 2012, *ApJ*, 757, 77
- Kratter, K. M. 2011, *ASPC*, 477, 47
- Kratter, K. M., Matzner, C. D., Krumholz, M. R., & Klein, R. *ApJ*, 708, 1585
- Looney, Leslie W., Mundy, L. G., & Welch, W. J. 2000, *ApJ*, 529, 477
- Mason, B. D., Henry, T. J., Hartkopf, W. I., ten Brummelaar, T., & Soderblom, D. R. 1998, *AJ*, 116, 2975
- Machida, M. N., Inutsuka, S., & Matsumoto, T. 2010, *ApJ*, 724, 1006

- Mathieu, R. D., Ghez, A. M., Jensen, E. L. N., & Simon, M. 2000, *prpl.conf*, 703
- Matsumoto, T., & Tomisaka, K. 2004, *ApJ*, 616, 266
- Maury, A. J., André, P., Hennebelle, P., Motte, F., Stamatellos, D., Bate, M., Belloche, A., Duchêne, G., & Whitworth, A. 2010, *A&A*, 512, 40
- Mellon, R. R., & Li, Z. -Y. 2008, *ApJ*, 681, 1356
- Mellon, R. R., & Li, Z. -Y. 2009, *ApJ*, 698, 922
- Myers, A. T., McKee, C. F., Cunningham, A. J., Klein, R. I., & Krumholz, M. R. 2012, *arXiv:1211.3467 Cosmic Physics*, vol. 9, 139
- Nakano, T., Nishi, R., & Umebayashi, T. 2002, *ApJ*, 573, 199
- Nakano, T., & Nakamura, T. 1978, *PASJ*, 30, 671
- Offner, S. S. R., Klein, R. I., McKee, C. F., & Krumholz, M. R. 2009, *ApJ*, 703, 131
- Offner, S. S. R., Kratter, K. M., Matzner, C. D., Krumholz, M. R. & Klein, R. I. 2010, *ApJ*, 725, 1485
- Klein, R., McKee, C. F., & Krumholz, M. R. 2009, *ApJ*, 703, 131
- O’Shea, B. W., Bryan, G., Bordner, J., Norman, M. L., Abel, T., Harkness, R., & Kritsuk, A. 2004, *astro-ph/0403044*
- Price, D. J., & Bate, M. R. 2007, *MNRAS*, 377, 77
- Raghavan, D., McAlister, H. A., Henry, T. J., Latham, D. W., Marcy, G. W., Mason, B. D., Gies, D. R., White, R. J., & ten Brummelaar, T. A. 2010, *ApJS*, 190, 1
- Reipurth, B., & Zinnecker, H. 1993, *A&A*, 278, 81
- Ruffert, M. 1994, *ApJ*, 427, 324
- Santos-Lima, R., de Gouveia Dal Pino, E. M., & Lazarian, A. 2012, *ApJ*, 747, 21
- Seifried, D., Banerjee, R., Klessen, R. S., Duffin, D., & Pudritz, R. E. 2011, *MNRAS*, 417, 1054
- Seifried, D., Banerjee, R., Pudritz, R. E., & Klessen, R. S. 2012, *MNRAS*, 423, 40
- Shatsky, N., & Tokovinin, A. 2002, *A&A*, 382, 92
- Shu, F. H. 1977, *ApJ*, 214, 488

- Tobin, J. J., Hartmann, L., Looney, L. W., & Chiang, H.-F. 2010, *ApJ*, 712, 1010
- Tokovinin A. A., & Smekhov, M. G. 2002, *A&A*, 382, 118
- Tomisaka, K. 1998, *ApJ*, 502. 163
- Troland, T. H., & Crutcher, R. M. 2008, *ApJ*, 680, 457
- Truelove, J. K., Klein, R. I., McKee, C. F., Holliman, J. H. II, Howell, L. H., & Greenough, J. A. 1997, *ApJ*, 489, 179
- Wang, P., & Abel, T. 2009, *ApJ*, 696, 96
- Wang, P., Li, Z. -Y., Abel, T., & Nakamura, F. 2010, *ApJ*, 709, 27
- Zhao, B., Li, Z. -Y., Nakamura, F., Krasnopolsky, R., & Shang, H. 2011, *ApJ*, 742, 10